Spatial Superchannel Routing in a Two-Span ROADM System for Space Division Multiplexing

L. E. Nelson, *Senior Member, IEEE*, M. D. Feuer, *Senior Member, IEEE*, K. Abedin, X. Zhou, *Senior Member, IEEE*, T. F. Taunay, J. M. Fini, *Member, IEEE*, B. Zhu, R. Isaac, R. Harel, G. Cohen, and D. M. Marom, *Senior Member, IEEE*

***Abstract*—We report a two-span, 67-km space-division-multiplexed (SDM) wavelength-division-multiplexed (WDM) system incorporating the first reconfigurable optical add–drop multiplexer (ROADM) supporting spatial superchannels and the first cladding-pumped multicore erbium-doped fiber amplifier directly spliced to multicore transmission fiber. The ROADM subsystem utilizes two conventional 1 × 20 wavelength selective switches (WSS) each configured to implement a 7 × (1 × 2) WSS. ROADM performance tests indicate that the subchannel insertion losses, attenuation accuracies, and passband widths are well matched to each other and show no significant penalty, compared to the conventional operating mode for the WSS. For 6 × 40 × 128-Gb/s SDM-WDM polarization-multiplexed quadrature phase-shift-keyed (PM-QPSK) transmission on 50 GHz spacing, optical signal-to-noise ratio penalties are less than 1.6 dB in Add, Drop, and Express paths. In addition, we demonstrate the feasibility of utilizing joint signal processing of subchannels in this two-span, ROADM system.**

***Index Terms*—Erbium-doped fiber amplifiers, optical fiber communication, optical fiber networks, wavelength routing.**

I. Introduction

OVER the decades-long history of optical communications, there has been a continual increase in the data transfer capacity of a single optical fiber, driving a reduction in the cost-per-bit delivered to end users, with a commensurate increase in total network traffic demand. The resulting Internet economy of applications enabled by abundant bandwidth has implications far beyond the optical communications industry itself. However, we are approaching saturation in the capacity of a single-mode fiber [1], as we fill the fiber's low-loss passband with data encoded using sophisticated modulation formats with near-optimal forward error correction (FEC) [2], [3]. Consequently, researchers are turning to space-division multiplexing (SDM), in which multiple data streams are carried in multiple transverse modes of an optical fiber that is not single-mode [4]. SDM has yielded dramatic increases in transmission capacity per fiber, using multiple modes in multimode fiber (MMF) [5]–[7], multiple cores in multicore fiber (MCF) [8]–[10], or multiple modes in multiple cores [11], [12]. However, capacity is only part of the picture; to sustain the future of the information economy, SDM must offer lower cost-per-bit, must offer a smooth transition from existing networks, and must support photonic routing at reconfigurable optical add/drop (ROADM) nodes as well.

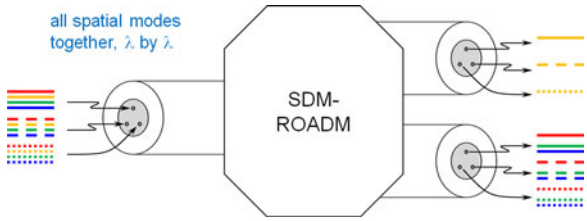

Fig. 1. Spatial superchannel routing in an SDM ROADM.

Spatial superchannels, in which high-rate (e.g., 1 Tb/s) data streams are transported as groups of subchannels occupying the same wavelength in separate modes/cores, can help lower the cost of transceivers through component sharing and simplified DSP [13]. Since all of the subchannels are routed together through the network, the approach also enables cost-effective ROADMs, in which a single switching element is used to route all of the subchannels belonging to a single superchannel. Spatial superchannel routing via an SDM ROADM is illustrated in Fig. 1. As long as the spatial superchannel comprises all of the spatial modes present at the given wavelength, the scheme also guarantees that the receiver at the end of the link will have all the information it needs to correct for possible mode mixing using digital signal processing (DSP). This is likely to be critical in MMF systems where strong mode mixing is omnipresent.

Optical amplifiers for multispan SDM systems must achieve the same beneficial cost scaling as transceivers and ROADMs, prompting research into multimode and multicore erbium-doped fiber amplifiers (MC-EDFAs) [14]–[17]. To take best advantage of MC-EDFA technology, such amplifiers should connect directly to multicore transmission spans and subsystems, since breakout devices to single-mode fiber at the amplifier inputs and outputs will add unwanted complexity, attenuation, and possibly

Manuscript received July 22, 2013; revised September 16, 2013; accepted September 18, 2013. Date of publication October 7, 2013; date of current version January 10, 2014.

L. E. Nelson and R. Isaac are with the AT&T Labs, Middletown, NJ 07748 USA (e-mail: lenelson@att.com; rejoy@research.att.com).

M. D. Feuer was with the AT&T Labs, Middletown, NJ 07748 USA. He is now with the Department of Engineering Science & Physics, C.U.N.Y. College of Staten Island, Staten Island, NY 10314 USA (e-mail: mark_feuer@ieee.org).

K. Abedin, T. F. Taunay, J. F. Fini, and B. Zhu are with the OFS Labs, Somerset, NJ 07733 USA (e-mail: kabedin@ofsoptics.com; ttaunay@ofsoptics.com; fini@ofsoptics.com; bzhu@ofsoptics.com).

X. Zhou was with the AT&T Labs, Middletown, NJ 07748 USA. He is now with Google, Inc., Mountain View, CA 94043 USA (e-mail: zhoux@ieee.org).

R. Harel and G. Cohen are with the Oclaro, Inc., Denville, NJ 07834 USA (e-mail: roey.harel@oclaro.com; Gil.Cohen@oclaro.com).

D. M. Marom is with the Hebrew University of Jerusalem, Jerusalem, Israel (e-mail: danmarom@mail.huji.ac.il).

Color versions of one or more of the figures in this paper are available online at http://ieeexplore.ieee.org.

Digital Object Identifier 10.1109/JLT.2013.2283912

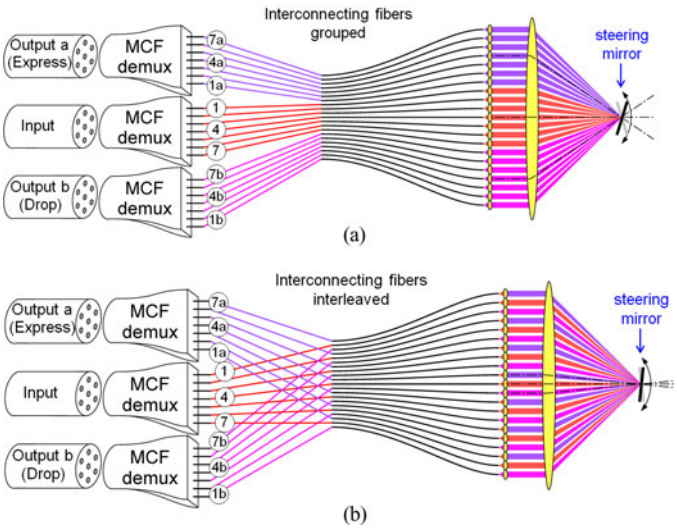

Fig. 2. Operating principle of $7 \times (1 \times 2)$ WSS. Type (a) has smaller spread of angles of incidence for the beams on the mirror, whereas type (b) offers smaller steering angles for the mirror.

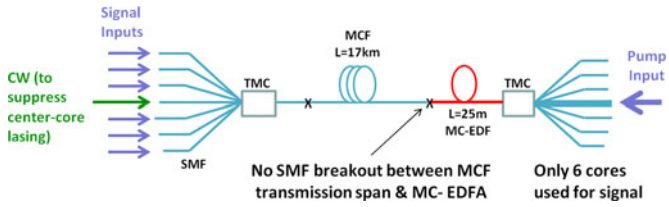

Fig. 3. Cladding-pumped multicore EDFA is directly spliced to multicore transmission span, eliminating the breakout to multiple single-mode fibers.

crosstalk. To share the power of a single multimode pump laser among all of the amplifying cores, cladding pumping similar to that developed for high-power fiber lasers [18] may be an attractive option.

In this paper, we present a detailed discussion of transmission and routing in a two-span ROADM transmission system adapted for spatial superchannels, expanding on the preliminary report in [19]. The ROADM subsystem comprises two 1×20 wavelength-selective switches (WSSs), with 18 fiber ports configured to support full Add/Drop/Express routing of six cores simultaneously, using only one steering mirror per wavelength in each WSS. At the ROADM input, a cladding-pumped MC-EDFA [16] is directly spliced to the MCF of the first transmission span, eliminating the cost and complexity of a breakout device as noted earlier. Our two-span transmission system was used to transport forty 50-GHz-spaced C-band wavelengths of 6×128 Gb/s each, and bit-error ratio (BER) was measured for each subchannel, as well as for the composite superchannel. BER performance suitable for systems with strong FEC was demonstrated for Add, Drop, and Express paths.

II. Experiment

Fig. 2 illustrates two possible ways to implement a $7 \times (1 \times 2)$ WSS by reprogramming a conventional 1×20 WSS [20], [21]. Instead of using a single WSS port for signal input, signals from seven cores of the input MCF are routed to ports 1 through 7 to reach the steering mirror at varying incidence angles. Depending on the mirror tilt, the beams are *jointly steered* to a set of output ports representing either the express or the drop path sets. Within a WSS, wavelengths are separated by a dispersive element (e.g., a diffraction grating, not shown in Fig. 2) and sent to separate WDM steering mirrors, effectively replicating the pattern of Fig. 2 for each wavelength. In this way, each mirror from the array of N mirrors can independently select paths for a particular wavelength superchannel and jointly switch the information from seven cores (or subchannels). In Fig. 2(a), the input ports are grouped (contiguously), whereas in Fig. 2(b), the input ports are interleaved in a perfect shuffle. The (b) arrangement allows the smallest possible steering angle for the mirror (required to switch by one port position in the conventional WSS; the minimal tilt angle is advantageous for beam steering technology), whereas the (a) arrangement offers a smaller spread in the angles of incidence of the beams striking the mirror. For this study, we adopted the grouped arrangement of Fig. 2(a). We used a commercial 1×20 WSS with MEMS mirrors for steering and a layer of liquid-crystal cells for controlling the attenuation [21]. The port assignments and the mirror tilt angles were chosen as needed to accomplish the $7 \times (1 \times 2)$ switching. The WSS channel spacing of 50 GHz matched that of our WDM signals. Our ROADM comprised two such WSSs in tandem in a switch-and-select configuration.

The cladding pumped MC-EDFA was directly spliced to the output of the first MCF transmission span, as shown in Fig. 3. The fusion-spliced test assembly comprised a tapered multicore coupler (TMC) fan-in device, a 17-km, seven-core MCF span, similar to that used in [22], a 25 m length of seven-core EDF with a core diameter of 3.2μm and a core pitch of 40μm, a TMC fan-out device, six single-mode output isolators to ensure stability (not shown in Fig. 3), and a high-power 980-nm multimode pump laser arranged for backward pumping. Because the MC-EDF had a different core pitch than the transmission MCF, a tapered multicore splice was used at the output end of the 17 km MCF span, as well as at the input end. As discussed in [16], the multifiber bundle of the TMC fan-out device included six singlemode fibers surrounding a single large-core MMF, which supplied the pump light. Because this central fiber is multimode, much of the pump light it supplies is released into the cladding (NA $= 0.45$) of the MC-EDF, where it serves to pump the six outer signal cores. However, this pumping scheme precluded use of the center core of the MC-EDF to carry data. Also, the central core of the MC-EDF experiences gain, so out-of-band CW light at 1562.5 nm was launched into the center core to suppress laser oscillation.

Our experimental diagram is shown in Fig. 4. The channel-under-test originates from an integrated tunable laser assembly (ITLA) with less than 100 kHz linewidth, whose output is sent to an integrated, polarization-multiplexed, quadrature modulator, driven with XI, XQ, YI, and YQ tributaries at 32 Gb/s to create a polarization-multiplexed quadrature phase-shift-keyed (PM-QPSK) data stream at 128 Gb/s. Delays and inversions

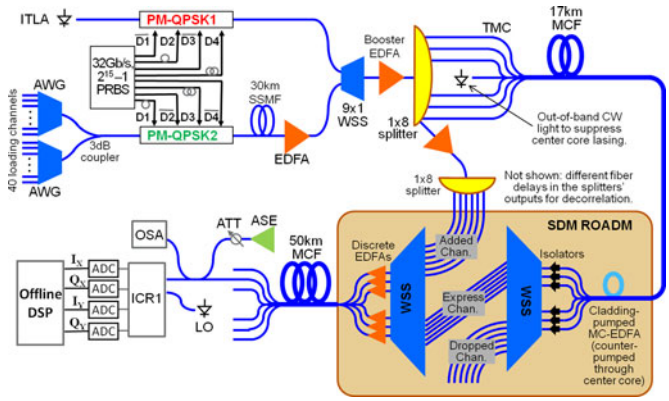

Fig. 4. Experimental setup for the two-span SDM ROADM system. AWG: arrayed waveguide grating multiplexer, PRBS: pseudo-random bit sequence, ATT: attenuator, OSA: optical spectrum analyzer, ADC: analog-to-digital converter.

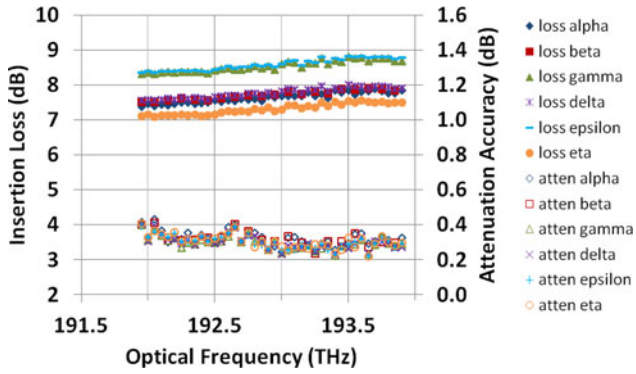

Fig. 5. ROADM insertion loss and attenuation accuracy for the Express path for all six subchannels. The "gamma" and "epsilon" connections utilize the nominal connections of the input WSS and the output WSS, respectively.

of the 32 Gb/s electrical data signals are used to assure decorrelation of the I and Q data sequences in both polarizations. A commercial 9×1 (50 GHz) WSS combines this channel with a 50-GHz spaced comb of 40 loading channels, also modulated with 128 Gb/s PM-QPSK data, and then, transmitted through 30 km of standard single-mode fiber (SSMF) for WDM channel decorrelation. A booster EDFA prepares the combined signals for launch into the first MCF span, and a 1×8 power splitter, along with the single ITLA for the superchannel-under-test, emulates a future integrated transmitter, where a single transmitter laser is shared among the spatial subchannels [13]. Decorrelation of the data signals carried by the spatial subchannels is achieved via the unmatched fiber lengths of the passive splitters' outputs and TMC inputs/outputs. As the ITLA was tuned through the 40 channels, the 9×1 WSS blocked the loading channel at the same wavelength and maintained a flat WDM spectrum at the booster EDFA output. The integrated MCF transmission span and ROADM preamplifier assembly of Fig. 3 follow the 1×8 splitter.

At the MC-EDF output, the second TMC splits out the cores to single-mode fibers to connect to the first of the two WSSs making up the ROADM subsystem. The WSS ports are connected as shown in Fig. 2(a) to accomplish the simultaneous Add, Drop, or Express path for all subchannels. (Note that in the rest of the paper, when discussing the system's Add, Drop, or Express path, we will refer to "spatial subchannels alpha, beta, gamma, delta, epsilon, and eta" instead of "cores," since the path through the ROADM contains single-mode fiber and no effort was made to maintain the same subchannel adjacencies in the two MCF spans.) Signals for the Add path are provided by amplifying and splitting the output from one remaining port of the first 1×8 splitter. After the SDM ROADM, discrete EDFAs boost the signal power before a third TMC at the input of the second MCF span. After the 50 km MCF span, a final TMC restores the signals to single-mode fibers for amplified spontaneous emission (ASE) addition and detection by an integrated coherent receiver (ICR) (21 GHz bandwidth) [23] with a second ITLA as local oscillator (LO). The ICR includes polarization diverse optical hybrids and four sets of high sensitivity balanced photodiodes with four differential linear amplifiers. Note that although all 40 channels are coincident at the receiver during the BER measurements, based on [23], we assume negligible penalty due to coincident-channel-interference. The receivers' outputs are digitized by a four-channel real-time oscilloscope with 80 GSa/s sampling rate and 33 GHz analog bandwidth and processed offline to compute BER over $\sim 1.6 \times 10^6$ bits of information for each spatial subchannel.

Frequencies of the 40 channels ranged from 191.95 to 193.90 THz (the long wavelength half of the C-band), and the launch powers into the TMCs for the first span and for the second span were set at -11 dBm/ch and $+5$ dBm/ch, respectively. The estimated loss of the module comprising the first MCF transmission span, the MC-EDFA background loss, and associated TMC's, tapers, and splices was $\sim$11–21 dB, suggesting that considerable improvement could be obtained with full optimization of the TMCs and tapered splices. The loss of the second span, including its TMCs, ranged from 18.8 to 23.3 dB for the various cores. As no amplification was utilized between the TMC outputs and ICR, the $+5$ dBm/ch launch power into the TMC inputs for the second span (i.e., $+21$ dBm total power at each discrete EDFA output) assured near optimal power [23] at the ICR for all cores. The loss of each WSS was $\leq$5 dB at all test wavelengths, and an additional 7 dB attenuation was applied in the second WSS to avoid overdriving the subsequent discrete ROADM postamplifiers. Power equalization among frequencies was implemented by adjusting the attenuation of the "Drop" WSS, as in a conventional ROADM system. Equalization among spatial subchannels was achieved by adjusting the gain of the ROADM postamplifiers.

The digital signal processing for the receiver is described in [13] and [24], with 13 T/2-spaced taps in the 2×2 time-domain-based adaptive equalizer for polarization multiplexing.

III. Results and Discussion

Performance tests of the SDM ROADM are presented in Figs. 5 and 6. It is worth noting that the $7 \times (1 \times 2)$ mode of WSS operation sketched in Fig. 2(a) exercises optical paths that are not used in conventional 1×20 mode, so these "ancillary connections" have not been fully verified in design and manufacture of the WSS. In particular, these connections

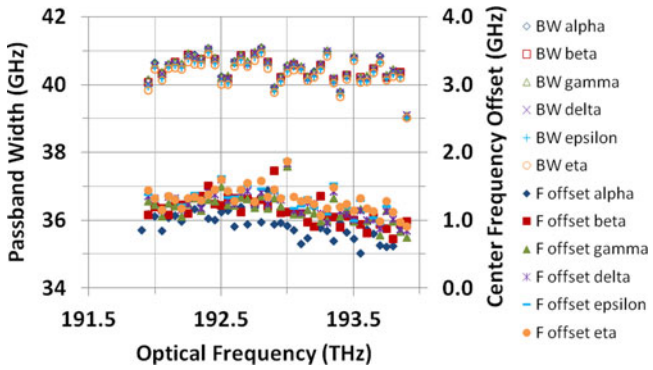

Fig. 6. ROADM passband width and center frequency offset for the Express path for all six subchannels. The "gamma" and "epsilon" connections utilize the nominal connections of the input WSS and the output WSS, respectively.

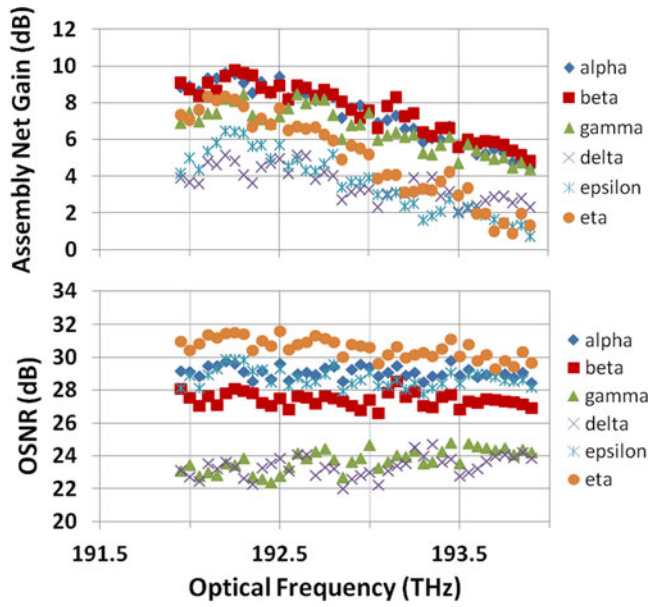

Fig. 7. Gain and OSNR (in 0.1 nm) for each core of the assembly comprising the 17-km MCF span, the MC-EDFA, and all associated tapers, splices, and TMCs.

operate in parallel, completing multiple port-to-port routing assignments by a single mirror. This further implies the optical power incident on each micromirror is six times greater than in the conventional operating mode. However, reflecting MEMS micromirrors are robust to these incident power levels. Fig. 5 compares the insertion losses of the SDM ROADM (i.e., two WSS in tandem without the loss contribution (and spread) of the TMC's) for all six subchannels, when the ROADM is set for Express with minimum attenuation. The subchannels are well-matched to each other and show no significant penalty for the ancillary connections, compared to the nominal optical path used in the conventional operating mode. The open symbols in Fig. 5 show the attenuation accuracy of the ROADM when it is set for 10 dB attenuation (i.e., 5 dB in the input WSS plus 5 dB in the output WSS). The combined attenuation error of ~0.3 dB is well within the device specifications, and there is no sign of deviations associated with the ancillary optical connections.

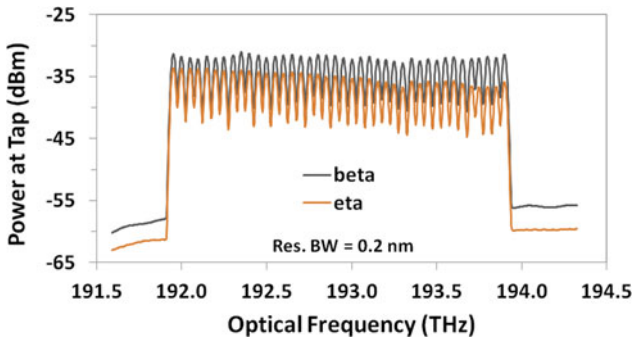

Fig. 8. The received power spectra after 67 km (Express Path) for the beta and eta subchannels, which are the highest-power and the lowest power cores, respectively.

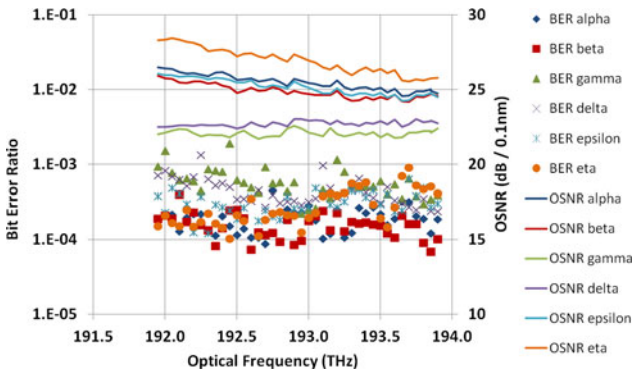

Fig. 9. The BER and received OSNR for all subchannels at all frequencies for the Express path without added ASE.

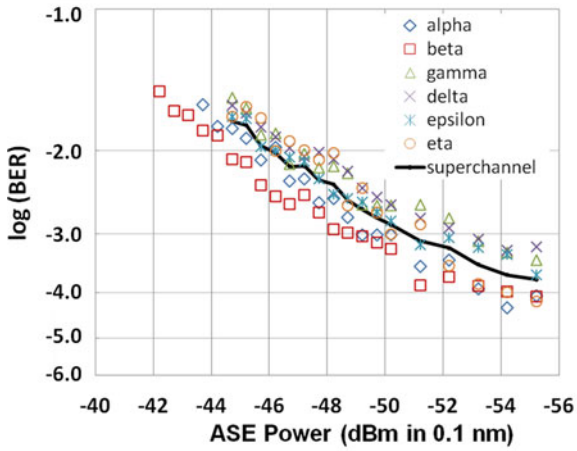

Fig. 10. Subchannel and superchannel BER as a function of added ASE loading power, for $f = 191.5$ THz for the Express path.

Fig. 6 presents ROADM performance tests in the frequency dimension, including the measured passband width and the measured center frequency offset from its ITU value. The passband widths were measured with a Yokogawa AQ6370 optical spectrum analyzer utilizing the WDM filter-peak analysis with 4 GHz resolution bandwidth, whereas the frequency offsets were measured with an Agilent 86122 A wavemeter utilizing the broad bandwidth algorithm. Although both parameters show

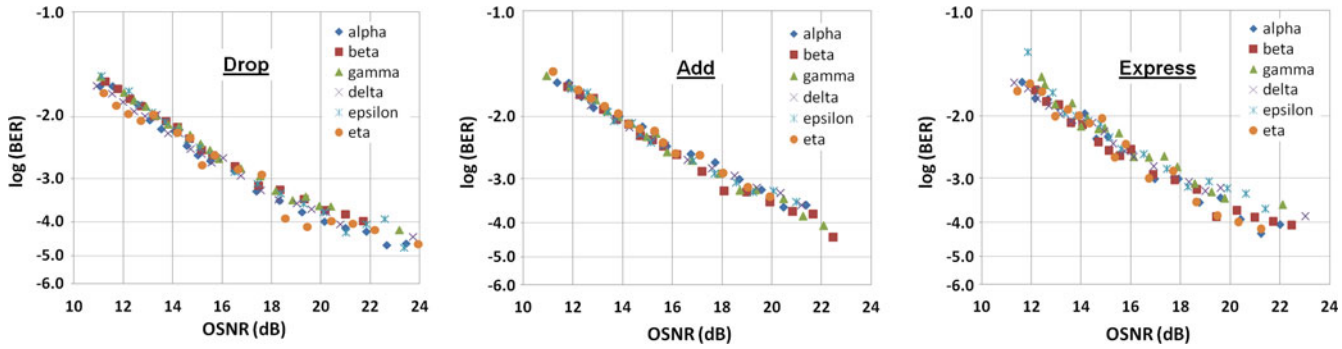

Fig. 11. Subchannel BERs as a function of OSNR for Drop (17 km), Add (50 km), and Express (67 km) paths, all six subchannels at 191.95 THz.

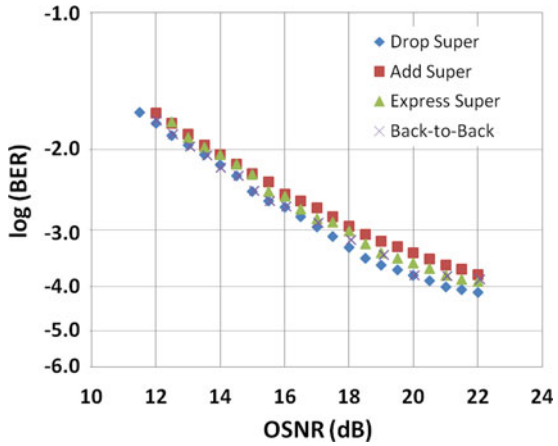

Fig. 12. Superchannel BER (average over the six subchannels) at $f = 191.95$ THz as a function of OSNR (in 0.1 nm) for Drop (17 km), Add (50 km), and Express (67 km) paths.

some slight variations over frequency, the differences among the six subchannels are negligible.

Fig. 7 shows the net gain of the assembly made up of the 17-km MCF span, the MC-EDFA, and associated tapered splices, as a function of optical frequency. As noted in [16], pumping efficiency of the cladding-pumped MC-EDFA was relatively low, limiting output power per core, and requiring operation under conditions of strong gain compression. Therefore, the gain and noise figure of the MC-EDFA were better at lower frequencies. The launch power of –11 dBm/ch at the TMC inputs of the 17 km MCF provided the best combination of OSNR, OSNR flatness, and net gain flatness for the entire assembly. The magnitude of the gain tilt varies significantly among the different cores, possibly due to varying splice losses at the input and output of the MC-EDFA. Optical time-domain-reflectometry measurements of the integrated assembly allow us to identify the core with the highest gain tilt (core eta, tilt $\sim$7 dB) as the core with the lowest-loss input splice, and thus, the highest input power and strongest gain compression. OSNR is more constant over frequency, but is generally lower for cores with high values of input loss.

Fig. 8 shows received power spectra at the output of the full two-span Express path for beta and eta subchannels, which correspond to the highest-power and lowest-power cores, respectively. The spectrum of the beta core is essentially flat, while the eta core shows a residual gain tilt of $\sim$2 dB, the largest of any of our subchannels. This illustrates one of the challenges of the SDM ROADM with one common mirror per wavelength: it is not possible for the ROADM to perfectly correct spectral tilt if different subchannels experience different tilt, as they do in this experiment with nascent technologies. In the future, improvements in the uniformity of the TMC insertion loss for the various ports and uniformity of the MC-EDFA gain will help to alleviate this challenge.

We have also measured BER for all 40 wavelengths and all subchannels for the express path at maximum OSNR condition, yielding the results shown in Fig. 9. Although there is some scatter in the data, the subchannels with the best OSNR generally show the lowest BER. For all subchannels and all wavelengths, the BER is less than 2×10^{-3}, which is well below the threshold of 2×10^{-2} required for full error correction using strong FEC with 24% coding overhead.

Considering that some variation among subchannels is inevitable, we note that it is not necessary for every subchannel to meet the FEC threshold, *if the FEC is applied to the superchannel as a whole*. For such superchannel-based FEC, "good" subchannels can partially compensate for "bad" subchannels, and it is only the aggregate BER of the whole that must fall below the FEC threshold. This is illustrated in Fig. 10, in which both individual subchannel BERs and the aggregate superchannel BER are plotted as functions of the added ASE power in 0.1 nm, for the Express path at $f = 191.95$ THz. (The data were plotted in this way because each subchannel has a different OSNR after transmission, and thus a different OSNR when a fixed amount of ASE loading is added during capture of data for BER versus OSNR curves.) Plotted in this way, the small variations among subchannels' output powers and OSNRs are seen to produce significant differences in the subchannel BERs, as we could expect to occur in deployed spatial superchannel systems. For an error threshold of 1×10^{-2}, the superchannel as a whole can tolerate $\sim$1 dB higher ASE loading than its weakest subchannel.

To verify the system performance along each of the routing paths, we have executed BER measurements for each subchannel in the Drop, Add, and Express paths, at the minimum frequency ($f = 191.95$ THz), the maximum frequency ($f = 193.90$ THz), and the center frequency ($f = 192.95$ THz).

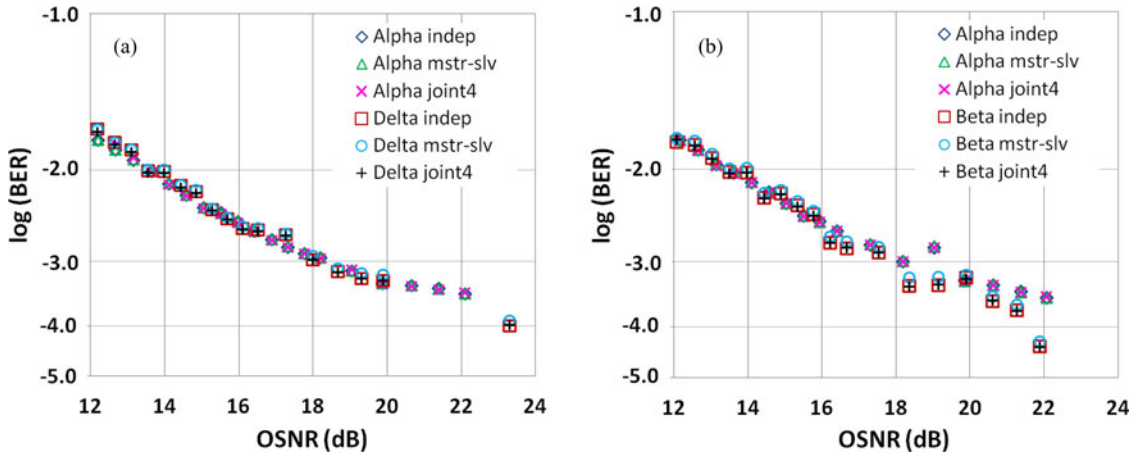

Fig. 13. Subchannel BERs as a function of OSNR for the Express path (two spans + ROADM) for two sets of two subchannels at 192.95 THz. There are three curves for each subchannel, comparing independent (indep) phase recovery to joint processing with master–slave (mast-slv) phase recovery and average phase recovery where the four phases from the X- and Y-polarizations of alpha and delta or beta are averaged (joint4). In (a), the relative delay of the alpha and delta subchannels for the Express path matched the relative delay of the LO paths to the alpha and delta receivers, whereas in (b) the alpha/beta delays were not matched.

Fig. 11 shows these BER measurements as a function of received OSNR (in 0.1 nm) for the channel at 191.95 THz. Considering each subchannel separately, the OSNR penalties at 1×10^{-2} BER (compared to a back-to-back measurement with the same transmitter and receiver) were <0.5 dB, <0.9 dB, and <0.9 dB, respectively, for the Drop, Add and Express paths. In similar measurements at the maximum frequency ($f = 193.90$ THz) and the center frequency ($f = 192.95$ THz), OSNR penalties <1.6 dB were observed for all subchannels.

To more clearly reveal the slight effects of fiber nonlinearity, we plot the superchannel (i.e., average over the six subchannels) BER as a function of received OSNR in Fig. 12. As expected, the relatively short Drop path shows the lowest penalty, while the Add and Express paths are approximately equal at 1×10^{-2} BER. At higher OSNR levels, the Add path shows slightly more penalty than the longer Express channel, possibly due to slightly different spectral tilts in the two cases.

IV. Joint Digital Signal Processing

As discussed in [13], spatial superchannels offer the possibility of utilizing joint signal processing of the subchannels by exploiting common-mode impairments to reduce the cost and power consumption of integrated receivers in space-division multiplexed networks. For two 112 Gb/s subchannels transmitted over a single 76 km MCF span, we showed that master–slave phase recovery reduced the DSP processing burden with no degradation of BER performance [13]. Here, we extend that work by investigating the feasibility of joint processing in a multispan ROADM system utilizing the setup of Fig. 4 with some augmentation. For these measurements, the signal from a second subchannel, after variable ASE-loading, was sent to a second receiver comprised of a second ICR and a four-channel real-time oscilloscope with 50 GSa/s sampling rate and 20 GHz analog bandwidth. The LO was split between the two receivers, as in [13]. We chose two sets of subchannels for joint processing: alpha and delta, and alpha and beta. The relative delay of the alpha and delta subchannels for the Express path was tuned with fiber jumpers to match the –4.6 ns (147 symbols) relative delay of the LO paths to the alpha and delta receivers. This ensured that the combined signal source and LO phase fluctuations received from the two different paths could be realigned using DSP. For comparison purposes, the relative delay of the alpha and beta subchannels for the Express path was 61.4 ns and was not matched to the (–4.6 ns) relative delay of the LO paths to the alpha and beta receivers.

The receivers' outputs were digitized and captured simultaneously for offline processing. The eight simultaneous signals (two orthogonal phase signals for each polarization from the two subchannels) were captured with 1M samples each. We used the same digital signal processing techniques as those described in [13], and the phase of each symbol was extracted by averaging over a window of 32 neighboring symbols. Fig. 13 shows a comparison of the BER versus OSNR curves for independent phase recovery, master–slave phase recovery (where the phase recovered from the X-polarization of alpha was used to demodulate the data measured from the Y-polarization of alpha and from the X- and Y-polarizations of delta or beta), and average phase recovery (where the four phases from the X- and Y-polarizations of alpha and delta or beta were averaged). Fig. 13 shows negligible differences among the BERs near 1×10^{-2} with independent and joint DSP (both for master–slave and average phase recovery). This appears true both for the case of matched relative delays (alpha/delta) and nonmatched relative delays (alpha/beta). Thus, we conclude that matched delay is not critical for this case of 100G PM-QPSK, where the LO and transmitter laser linewidths are less than 100 kHz, which is one order of magnitude lower than the tolerance for feed-forward phase recovery. At lower BERs (below 1×10^{-3}), the BER for master–slave phase recovery is slightly worse than for independent or average phase recovery for the delta and beta subchannels, which is reasonable.

Although equipment availability prevented us from simultaneously capturing more than two subchannels, we believe that joint DSP utilizing a phase based on the average of more than two subchannels would further improve the phase

accuracy. The hardware effort for phase recovery may be relatively small in an ultralong-haul system compared to that for large CD-compensating filters; however, phase recovery can contribute to a significant portion of overall DSP effort for metro or regional systems, especially when using a high-order modulation format (the required hardware effort for phase recovery increases as modulation order increases). In addition, phase recovery is only one example of the joint processing possible with spatial superchannels. For example, although joint processing cannot help to reduce DSP effort for CD *compensation*, it can reduce the effort for CD *estimation*, when the CD estimate obtained for a single subchannel is utilized for the other spatial subchannels.

V. Conclusion

We demonstrated transmission and routing of 6 core $\times$ 40λ $\times$ 128-Gb/s SDM-WDM-PM-QPSK signals in a two-span, 67-km, MCF system including a ROADM adapted for spatial superchannels, and measured its BER performance. A cladding-pumped multicore-EDFA was directly spliced to the first MCF transmission span, obviating the need for a pair of MCF-to-SMF breakout devices. The WSS-based SDM ROADM successfully steered six spatial subchannels jointly with each of its WDM mirror elements, enabling full Add/Drop/Express capability for all wavelengths, and measurements showed insignificant differences in the subchannel insertion losses, attenuation accuracies, and passband widths, compared to the conventional operating mode for the WSS. In addition, we demonstrated the feasibility of joint processing in the two-span, ROADM system by measuring negligible differences among the BERs with independent and average phase recovery.

Acknowledgment

We gratefully acknowledge S. Woodward and P. Magill of AT&T Labs and D. DiGiovanni of OFS Labs for their advice and support. In addition, we thank NeoPhotonics for the loan of the integrated coherent receivers.

References

[1] R. J. Essiambre and R. W. Tkach, "Capacity trends and limits of optical communication networks," *Proc. IEEE*, vol. 100, no. 5, pp. 1035–1055, May 2012.

[2] F. Chang, K. Onohara, and T. Mizuochi, "Forward error correction for 100G transport networks," *IEEE Commun. Mag.*, vol. 48, no. 3, pp. 48–55, Mar. 2010.

[3] T. Mizuochi, T. Sugihara, Y. Miyata, K. Kubo, K. Onohara, S. Hirano, H. Yoshida, T. Yoshida, and T. Ichikawa, "Evolution and status of forward error correction," presented at the Optical Fiber Communication-Nat. Fiber Optical Engineers Conf., Los Angeles, CA, USA, Mar. 2012, paper OTuA2.6.

[4] D. J. Richardson, J. Fini, and L. E. Nelson, "Space-division multiplexing in optical fibres," *Nature Photon.*, vol. 7, pp. 354–362, May 2013.

[5] V. A. J. M. Sleiffer *et al.*, "73.7 Tb/s (96 $\times$ 3 $\times$ 256-Gb/s) mode-division-multiplexed DP-16QAM transmission with inline MM-EDFA," presented at the Eur. Conf. Optical Communication, Amsterdam, Netherlands, Sep. 2012, paper Th.3.C.4.

[6] R. Ryf *et al.*, "32-bit/s/Hz spectral efficiency WDM transmission over 177-km few-mode fiber," presented at the Optical Fiber Communication-Nat. Fiber Optical Engineers Conf., Anaheim, CA, USA, Mar. 2013, paper PDP5 A.1.

[7] E. Ip *et al.*, "146λ $\times$ 6 $\times$ 19 Gbaud wavelength- and mode-division multiplexed transmission over 10 $\times$ 50-km spans of few mode fiber with a gain-equalized few-mode EDFA," presented at the Optical Fiber Communication-Nat. Fiber Optical Engineers Conf., Anaheim, CA, USA, Mar. 2013, paper PDP5 A.2.

[8] J. Sakaguchi *et al.*, "19-core fiber transmission of 19 $\times$ 100 $\times$ 172-Gb/s SDM-WDM-PDM-QPSK signals at 305 Tb/s," presented at the Optical Fiber Communication-Nat. Fiber Optical Engineers Conf., Los Angeles, CA, USA, Mar. 2012, paper PDP5 C.1.

[9] H. Takara *et al.*, "1.01-Pb/s (12 SDM/222 WDM/456 Gb/s) crosstalk-managed transmission with 91.4-b/s/Hz aggregate spectral efficiency," presented at the Eur. Conf. Optical Communication, Amsterdam, Netherlands, Sep. 2012, paper Th3.C.1.

[10] H. Takahashi *et al.*, "First demonstration of MC-EDFA-repeatered SDM transmission of 40 $\times$ 128-Gbit/s PDM-QPSK signals per core over 6,160-km 7-core MCF," presented at the Eur. Conf. Optical Communication, Amsterdam, Netherlands, Sep. 2012, paper Th.3.C.3.

[11] C. Xia, R. Amezcua-Correa, N. Bai, E. Antonio-Lopez, D.M. Arrioja, A. Schulzgen, M. Richardson, J. Liñares, C. Montero, E. Mateo, X. Zhou, and G. Li, "Hole-assisted few-mode multicore fiber for high-density space-division multiplexing," *IEEE Photon. Technol. Lett.*, vol. 24, no. 21, pp. 1914–1916, Nov. 1, 2012.

[12] D. Qian *et al.*, "1.05 Pb/s Transmission with 109b/s/Hz spectral efficiency using hybrid single- and few-mode cores," presented at the Frontiers in Optics Conf., Rochester, NY, USA, Oct. 2012, paper FW6 C.3.

[13] M. D. Feuer, L. E. Nelson, X. Zhou, S. L. Woodward, R. Isaac, B. Zhu, T. F. Taunay, M. Fishteyn, J. M. Fini, and M. F. Yan, "Joint digital signal processing receivers for spatial superchannels," *IEEE Photon. Technol. Lett.*, vol. 24, no. 21, pp. 1957–1960, Nov. 1, 2012.

[14] P. M. Krummrich, "Optical amplification and optical filter based signal processing for cost and energy efficient spatial multiplexing," *Opt. Exp.*, vol. 19, no. 17, pp. 16636–16652, Aug. 15, 2011.

[15] Y. Jung *et al.*, "First demonstration of multimode amplifier for spatial division multiplexed transmission systems," presented at the Eur. Conf. Optical Communication, Geneva, Switzerland, Sep. 2011, paper Th.13.K.4.

[16] K. Abedin *et al.*, "Cladding-pumped erbium-doped multicore fiber amplifier," *Opt. Exp.*, vol. 20, no. 18, pp. 20191–20200, Aug. 27, 2012.

[17] Y. Mimura *et al.*, "Batch multicore amplification with cladding-pumped multicore EDFA," presented at the Eur. Conf. Optical Communication, Amsterdam, Netherlands, Sep. 2012, paper Tu.4.F.1.

[18] D. DiGiovanni and A. J. Stentz, "Tapered fiber bundles for coupling light into and out of cladding-pumped fiber devices," U.S. Patent 5 864 644, 1999.

[19] M. D. Feuer *et al.*, "ROADM system for space division multiplexing with spatial superchannels," presented at the Optical Fiber Communication-Nat. Fiber Optical Engineers Conf., Anaheim, CA, USA, Mar. 2013, paper PDP5B.8.

[20] D. M. Marom, D. T. Neilson, D. S. Greywall, C. S. Pai, N. R. Basavanhally, V. A. Aksyuk, D. O. López, F. Pardo, M. E. Simon, Y. Low, P. Kolodner, and C. A. Bolle, "Wavelength-selective 1 $\times$ K switches using free-space optics and MEMS micromirrors: Theory, design, and implementation," *IEEE J. Lightw. Technol.*, vol. 23, no. 4, pp. 1620–30, Feb. 15, 2005.

[21] U. Arad, Y. Corem, B. Frenkel, V. Deich, J. Dunayevsky, R. Harel, P. Janosik, G. Cohen, and D. M. Marom, "MEMS wavelength-selective switch incorporating liquid crystal shutters for attenuation and hitless operation," presented at the Optical MEMS Nanophotonics Conf., Kanazawa, Japan, Aug. 2013, paper TA-S2.4.

[22] B. Zhu *et al.*, "112-Tb/s space-division multiplexed DWDM transmission with 14-b/s/Hz aggregate spectral efficiency over a 76.8-km seven-core fiber," *Opt. Exp.*, vol. 19, no. 17, pp. 16665–16671, Aug. 15, 2011.

[23] L. E. Nelson *et al.*, "Colorless reception of a single 100 Gb/s channel from 80 coincident channels via an intradyne coherent receiver," in *Proc. IEEE Photon. Conf. 2012*, Burlingame, CA, USA, Sep. 2012, paper TuE4.

[24] X. Zhou, J. Yu, M. F. Huang, Y. Shao, T. Wang, L. Nelson, P. Magill, M. Birk, P. I. Borel, D. W. Peckham, R. Lingle, and B. Zhu, "64-Tb/s, 8 b/s/Hz, PDM-36QAM transmission over 320 km using both pre- and post-transmission digital signal processing," *J. Lightw. Technol.*, vol. 29, no. 4, pp. 571–577, Feb. 15, 2011.

Authors' biographies not available at the time of publication.